Minibasin depocentre migration during diachronous salt welding, offshore Angola

Zhiyuan Ge[a]*, Rob L. Gawthorpe[a], Atle Rotevatn[a], Leo Zijerveld[a], Christopher A-L. Jackson[b] and Ayodeji Oluboyo[a,c,d]

[a]*Department of Earth Science, University of Bergen, Allégaten 41, 5007 Bergen, Norway*
[b] *Basins Research Group (BRG), Department of Earth Science & Engineering, Imperial College, Prince Consort Road, London, SW7 2BP, UK*
[c] *School of Earth, Atmospheric and Environmental Sciences, University of Manchester, Manchester, UK*
[d] *PGS-Reservoir, Weybridge, UK*

*Correspondance e-mail: Zhiyuan.Ge@uib.no

ABSTRACT

Salt tectonics is an important part of the geological evolution of many continental margin salt basins, yet the four-dimensional evolution of the minibasins, the fundamental building block of these and many other salt basins, remains poorly understood. Using high-quality 3D seismic data from the Lower Congo Basin, offshore Angola, we document the dynamics of minibasin subsidence at a scale of tens of kilometres. We show that, during the Albian, a broadly tabular layer of carbonate was deposited prior to substantial salt flow, diapirism, and minibasin formation. We identify four subsequent stages of salt-tectonics and related minibasin evolution: (i) Cenomanian to Coniacian gravity-driven extension, driven by basinward tilting of the salt layer, and the formation of low-displacement normal faults and related salt rollers. During this stage, local salt welding led to the along-strike migration of fault-bound depocentres; (ii) Santonian to Paleocene salt welding below the eastern part of the minibasin caused a westward shift in depocentre location; (iii) Eocene to Oligocene welding below the minibasin centre, caused formation of a turtle and an abrupt shift of depocentres towards the immediate margins of the flanking salt walls; and (iv) a Miocene to Holocene eastward shift in depocentre location due to regional tilting, contraction, and diapir squeezing. Our study shows that salt welding and subsequent contraction are key controls on minibasin geometry, subsidence and stratigraphic patterns. In particular, we show how salt welding is a protracted process, spanning over 70 Myr of salt-tectonic history, with these dynamics recorded in the progressive migration of minibasin depocentres. The variations of minibasin growth and salt flow and welding have implications for geometrical and geomorphological evolution, sediment dispersal as well as salt-related structure growth during minibasin evolution.

Keywords minibasin, depocentre migration, salt weld, salt tectonics, passive margin, offshore Angola

1. Introduction

A minibasin is a syn-kinematic succession of sediment that subsides into a body of salt (M. P. Jackson & Talbot, 1991; Peel, 2014). Minibasins are commonly found in passive margin salt basins, such as the Gulf of Mexico (e.g. Hudec, Jackson, Vendeville, Schultz-Ela, & Dooley, 2011; Lamb, Toniolo, & Parker, 2006; Prather, Booth, Steffens, & Craig, 1998), the West African margin (e.g. Hudec & Jackson, 2004; Marton, Tari, & Lehmann, 2000) and the Brazil margin (e.g. Quirk et al., 2012), as well as cratonic salt basins such as the Zechstein (e.g. Hodgson, Farnsworth, & Fraser, 1992) and Precaspian basins (e.g. Barde et al., 2002; Duffy et al., 2017). Most studies have focused on the geometry and evolution of salt-related structures flanking the minibasins (e.g. diapirs) rather than the minibasins themselves. As a consequence of this, certain subsidence dynamics of the minibasins are not fully understood (e.g. Brun & Fort, 2011; Clark, Stewart, & Cartwright, 1998; Hudec & Jackson, 2007; Peel, 2014; Rowan, Peel, & Vendeville, 2004; Rowan & Weimer, 1998; Trudgill, 2011; B. C Vendeville & Jackson, 1992).

Current models of the minibasin initiation and subsidence have been studied using subsurface data (e.g. Hudec, Jackson, & Schultz-Ela, 2009; McBride, Rowan, & Weimer, 1998), numerical modelling (e.g. Goteti, Ings, & Beaumont, 2012; Peel, 2014), and scaled physical experiments (e.g. Callot, Salel, Letouzey, Daniel, & Ringenbach, 2016; Fort, Brun, & Chauvel, 2004; M. P. A Jackson & Vendeville, 1994; Warsitzka, Kley, & Kukowski, 2013). Essentially, a minibasin forms as a package of sediments sinks into underlying salt, which is mobilized and evacuated into adjacent salt highs. Subsidence may be driven by either sediment loading, extension or contraction (e.g. Hudec et al., 2009; Peel, 2014). As a minibasin sinks into the underlying salt, the salt is gradually depleted, and ultimately, the minibasin comes into contact with the sub-salt strata, creating a salt weld (Martin P. A Jackson & Cramez, 1989; M. P. A Jackson & Vendeville, 1994). After welding, salt mobilization is no longer a viable mechanism to accommodate further subsidence of the minibasin (Martin P. A Jackson & Hudec, 2017). However, such conceptual model of minibasin growth oversimplifies the heterogeneities existed in passive margin salt basins where direction and amount of sediment supply, location of minibasin initiation and salt thickness are all variable. As a result, how minibasin subside and weld on sub-salt in 3D is still unclear. Moreover, as minibasin subsidence and subsequent salt weld have a direct impact on formation of related salt structures, a better understanding of minibasin evolution and growth also improves our knowledge on the development of salt-related structures in such settings.

The main aims of this analysis is to understand the relationship between minibasin development and salt flow and weld and how they interact in 3D. We have chosen a single minibasin where the seismic dataset has best quality and wide coverage along strike among a series

of elongate minibasins within the Lower Congo Basin. The high quality, well-calibrated 3D reflection seismic dataset has allowed us to carry out a detailed tectono-stratigraphic analysis of the three-dimensional growth of the selected minibasin (Fig. 1).

2. Geological setting

The Lower Congo Basin formed during the opening of the South Atlantic Ocean, following early Cretaceous rifting and breakup of the Gondwana super-continent (e.g. Nürnberg & Müller, 1991). After rifting, an up to 1 km thick evaporite sequences was deposited in the late Aptian (Loeme Formation) during a marine transgression and a subsequent period of basin isolation and desiccation (Fig. 2) (Anderson, Cartwright, Drysdall, & Vivian, 2000; Lavier, Steckler, & Brigaud, 2001). After salt deposition, a shallow marine clastic-carbonate succession (Pinda Group) was deposited in Albian; this unit records the beginning of open marine conditions along the margin (Anderson et al., 2000; Marton et al., 2000; Valle, Gjelberg, & Helland-Hansen, 2001).

From Albian times onward, margin tilting triggered salt mobilization and drove basin-wide salt tectonics, which is characterized by thin-skinned deformation of the cover strata overlying the Loeme salt. In detail, three structural domains are identified; updip and downdip domains of extension and contraction, respectively, separated by a domain of translation (Fort et al., 2004; Marton et al., 2000). From the Santonian until the Eocene, the shale-dominated Iabe and Landana formations occurred as salt diapirs grew and minibasins subsided into the mid-slope translational domain (Anderson et al., 2000; Marton et al., 2000; Valle et al., 2001) (Fig. 2). The Oligocene Malembo Formation consists mainly of claystone interbedded with sandstone-rich turbidites (Anderson et al., 2000; Valle et al., 2001), with the increase in siliciclastic sediment being closely linked to the development of the Congo deepwater fan (Anka & Séranne, 2004). Miocene deepwater deposition was increasingly confined by the bathymetric highs created by squeezed salt diapirs due to contraction associated with regional uplift of the margin (Oluboyo, Gawthorpe, Bakke, & Hadler‐Jacobsen, 2014). From the Pliocene onwards, silty and muddy sediments were deposited in the Lower Congo Basin as the Congo fan delivered sediment to the northern part of the basin (Fig. 2) (Anka & Séranne, 2004; Valle et al., 2001).

3. Data and methods

3.1 Seismic and well data

This study utilises a high-quality, pre-stack time-migrated, three-dimensional seismic survey with a record length of six seconds two-way travel time (TWT), and inline and crossline spacing of 50 m. The seismic data are displayed with SEG normal polarity, where a downward increase in acoustic impedance is represented by a peak and is coloured in red in the displayed seismic

profiles. The data quality is excellent in the interval of interest, although it diminishes on the flanks of salt diapirs due to the presence of steeply dipping, upturned minibasin strata in those areas. The average vertical seismic resolution ranges from 30 to 60 m, with main frequency falling between 20–40 Hz and assuming a seismic velocity of 3000 m/s (e.g. Birch, 1960). Two proprietary nearby wells containing conventional well-log data (e.g. gamma ray, sonic) as well as published age schemes provid some age constraints for our mapped seismic horizons (Anderson et al., 2000; Valle et al., 2001).

3.2 Seismic interpretation

Thirteen horizons were mapped across the study area on the basis of stratal terminations and major changes in seismic facies (Fig. 2). The horizons can be readily identified in the seismic dataset throughout the study area. The average interval between two horizons is 150-300 ms TWT up to Eocene, which corresponds to 225–450 m assuming a seismic velocity of 3000 ms^{-1}. From Paleocene and onwards, the average interval velocity is from 400 to 800 ms TWT. The base and top salt horizons delimit the Loeme salt, whereas the top salt and top Albian horizons bound a pre-kinematic succession deposited before the onset of major salt tectonics. The syn-kinematic interval, which records salt diapir growth and minibasin subsidence, extends from the top Albian to the seafloor (Fig. 2). Following existing convention, all strata above top salt are referred as 'supra-salt cover', and strata beneath base salt are referred to as 'sub-salt strata'. The interpreted horizons allow sub-division of the supra-salt succession into eleven stratal units (Fig. 2).

3.3 Time-thickness, cross-sections and salt weld

We calculated TWT thickness (isochron) maps of all 11 supra-salt stratigraphic units; thickness changes in these units, in conjunction with stratal geometries and seismic facies, are inferred to record spatial variations in salt-driven minibasin subsidence. One potential pitfall of this method relates to errors in the thickness calculations that could result from steeply dipping strata and lateral velocity variations (Marsh, Imber, Holdsworth, Brockbank, & Ringrose, 2010; Oluboyo et al., 2014). We have mitigated this by carefully cross-checking isochrons with the seismic sections to ensure thickness changes observed in one are observed in the other. A second potential problem relates to uncertainties in defining the geometry of a depocentre, since the depocentre is represented simply by a relatively thick part of a specific stratigraphic interval. To better constrain depocentre geometry, we define depocentres as the area corresponding to the upper 30% thick of the studied stratigraphic interval; contour lines with 50 or 100 ms TWT increment are used to illustrate depocentre location.

Previous studies have indicated that it is difficult to completely remove salt from a salt weld

(Bryce Hedrick Wagner, 2010; Bryce H Wagner & Jackson, 2011) and, in practice, salt welds can contain tens of metres of remnant salt (C. A.-L. Jackson, Rodriguez, Rotevatn, & Bell, 2014; Rowan, Lawton, & Giles, 2012; Bryce Hedrick Wagner, 2010). Therefore, a seismically apparent weld may have up to 50 m of remnant salt (Bryce H Wagner & Jackson, 2011). To quantitatively constrain the location of salt weld, we infer a weld where top and base salt horizons are less than 25 ms TWT apart, i.e. approximately 50 m assuming a seismic velocity of 4000 m/s (e.g. Birch, 1960). A key assumption in our analysis is that the timing of salt welding can be estimated by variations in stratal thickness. More specifically, as a minibasin starts to weld, strata thin vertically upward, and the geometry of stratigraphic interval changes from bowl or wedge shape to layers with limited thickness variation (Fig. 1d) (Martin P. A Jackson & Hudec, 2017; Rowan & Weimer, 1998).

4. Present day structural style and salt distribution

The studied minibasin trends NNE, and is up to 16 km wide and 56 km long (Figs 1B, 3–5). The minibasin is thickest in the southwest, with strata thinning and being upturned against flanking diapirs that are up to 2000 ms TWT tall (Figs 3, 4 and 5).

Salt is generally very thin (<25 ms TWT) below the minibasin, suggesting a large part of the minibasin is welded to subsalt strata. Locally, however, three broadly NE-trending salt-related structures occur below the minibasin; these salt-related structures are up to 600 ms TWT thick, 6 km wide, and 17 km long (X–Z; Fig. 3c and d). Among them, salt pillows X and Y locate in the northeast and centre of the minibasin respectively (Fig. 3d), and Salt Roller Z is bounded on its western side by a moderate throw (400 ms TWT), NW-dipping normal fault (Fig. 5b).

5. Supra-salt structural style and stratigraphic architecture

Strata preserved within the minibasin shows significant temporal and spatial variations in geometry and thickness. The Albian succession, which sits directly on top of the salt with limited thickness variations, is regarded as pre-kinematic (Fig. 7a). Subsequent minibasin development can be divided into four stages, based on stratal geometry and the relative locations of the depocentres.

i) Cenomanian to Coniacian: Depocentre initiation and lateral migration (Fig. 7b-d)

ii) Santonian to Paleocene: Transverse shift to the west (Fig. 7e and f)

iii) Eocene to Oligocene: Turtle structure formation (Fig. 7g and h)

iv) Miocene to present day: Transverse migration crossing underlying salt pillows (Fig. 7i-k)

5.1. Albian

Description. The Albian succession is generally thin and tabular, with an average thickness of *c*. 100 ms TWT (Figs 4 and 5). Thickness changes are gradually across the study area (Fig. 7a). The only relatively thick part is in the northwest, where it is over 300 ms TWT (Fig. 7a).

Interpretation. The absence of major thickness variations suggests that the Albian was a tectonically quiescent stage. Little deformation occurred during this period, suggesting the gravity-driven thin-skinned salt tectonics has not widely commenced in the study area (Fig 7a). However, local thickness variation indicates some passive diapirism may already exist (Figs 4a and 9a).

5.2 Cenomanian to Coniacian

Description. Small-scale normal faults, which are spaced 1–4 km and 3–5 km long, and that have up to 100 ms TWT fault throw, offset the Cenomanian to Coniacian succession (Figs 4 and 5). During the Cenomanian, the first major minibasin depocentre (D1) developed in the north of the study area (Fig 7b). The depocentre was c. 27 km long and c. 1.6 km wide (Fig. 4). In its northern part, its eastern boundary is defined by an abrupt thickness change over 100 ms TWT, indicating a syn-depositional growth fault (F1; Figs 4a and 7b).

Two depocentres, which are markedly offset from the Cenomanian depocentre (D1), characterise the Turonian interval (D2a and D2b; Fig. 7c). The northern depocentre (D2a) is relatively small (c. 6 km long and c. 6 km wide; Fig. 7c) and offset 2 km east of the one defined in the underlying, Cenomanian succession (D1), lying immediately west of Salt Pillow X (Figs 4a and 8a). Depocentre D2b is c. 27 km long and c. 7 km wide, and is located against the eastern salt wall in the central part of the minibasin (Fig. 7c). A seismic profiles shows the depocentre defines a south-eastwards-thickening wedge expanding from less than 100 ms TWT in the northwest to approximately 300 ms TWT in southeast, documenting asymmetric subsidence linked to extension and ongoing salt flow and diapirism (Fig. 5a). Specifically, the thickening towards southeast indicates the withdrawal of more salt from southeast relative to the northwest (Fig. 5a). Moreover, onlap onto the top Cenomanian within Depocentre D2b suggests in the along strike migration of the Depocentre D2b over Depocentre D1 (Fig. 6).

We distinguish three depocentres in the Coniacian interval; these are all offset to the southeastern side of the Turonian depocentres (Fig. 7d). Depocentre D3a migrated to the east relative to depocentres D1 and D2a, lying on the eastern side of Salt Pillow X (Figs 4a and 8a). Depocentre D3b is located against the eastern salt wall and partly coincides with the underlying depocentre (D2b) but extends further to the south bounding Salt Pillow Y in the east and south (Figs 5, 6 and 7d). Depocentre D3c is approximately 1 km wide and 8–10 km long and occurred

along the western boundary of Salt Roller Z (Fig. 5b). In cross section, depocentres D3b and D3c are both composed of growth wedges thickening from less than 100 ms TWT in the southwest to over 200 ms TWT in the east, suggesting asymmetrical subsidence and salt flow (Fig. 5b). In other parts of the minibasin, normal faulting had largely ceased and the extension was mainly accommodated by salt diapism as indicated by the triangle shape of salt diapirs (Figs 4b, 5a and 9d) (sensu Martin P. A Jackson, Vendeville, & Schultz-Ela, 1994).

Interpretation. Overall, the Cenomanian to Coniacian succession is characterized by the initiation and lateral migration of depocentres (Fig. 8a). Depocentres developed during this stage are generally related with extension and normal faulting. For example, depocentres D1-D3c thicken towards normal faults and extensional diapirs, which are thus inferred to be active at this time (Figs 4 and 5). Our local evidence for Cenomanian to Coniacian extension is consistent with regional evidence provided by (Valle et al., 2001), who relate extension to thin-skinned gravity gliding of supra-salt cover in response to regional tilting.

Minibasin subsidence also initiated salt depletion and subsequent welding. For example, Depocentres D1 and D2b were superposed (Fig. 4a) because there was sufficient salt beneath the northern corner of Depocentre D1 to allow continued subsidence. In contrast, by D2 times (i.e. Turonian), the southern part of Depocentre D1 had welded, with salt having flowed laterally into embryonic diapirs flanking the minibasin (Fig. 9c and d). As a result, subsidence shifted along strike towards the south into a location where salt was still relatively thick and accommodation generation, driven by salt expulsion, was still ongoing (Fig. 8e). This is evident by the Turonian strata laterally onlapping over the Cenomanian strata in the Depocentre D1 area (Fig. 6). A similar process occurred in the Coniacian, when subsidence again shifted progressively along strike to the south (i.e. D3a and D3b are offset from depocentres D2a and D2b); we again infer this shift occurred in response to the onset of (local) welding (Figs 6, 7c and 8a). The inferred place of salt weld generally had 500-700 ms TWT thick supra-salt cover when welding occurred (e.g. Fig. 5), which is in a good agreement with the initial salt thickness of c. 1 km assuming a seismic velocity of 3000 ms^{-1}.

Progressive depocentre migration and related salt welding were also responsible for the formation of the salt pillows, with these remnant, albeit relatively thick salt bodies being trapped below the subsidising minibasin (e.g. D2a and D3a bounding Salt Pillow X; Fig. 4).

5.3. Santonian to Paleocene

Description. The Santonian times saw an abrupt westward shift in subsidence (D4a and D4c; Fig.

7e). In the northern part of the study area, two depocentres developed on the western and eastern side of Salt Pillow X (D4a and D4b; Fig. 4a). The cross-section shows that the Depocentre D4a strata thin outwards from the middle over 260 ms TWT towards its flanks of less than 100 ms TWT, with the salt-cored anticline underlain by pillow X (Fig. 4a). In contrast, Depocentre D4b developed above, but is noticeably smaller than, Depocentre D3a (Fig. 4a). Further south, 260 ms TWT thick, Depocentre D4c developed in the western part of the minibasin, bounded by Salt Pillow Y and the western salt wall (Fig. 5a). A minor exception to the broadly westward shift in subsidence is represented by Depocentre D4d, which is developed in the southeast above Depocentre D3b (Fig. 5b).

From the Campanian until the Paleocene, the subsidence regime was broadly similar to that characterising the Santonian (Fig. 7f). Depocentres D5a, D5b and D5c formed above D4a, D4c and D4d, respectively (Fig. 7d), with the main difference being that Depocentre D5a (3–4 km long and 1–2 km wide) was smaller than depocentre (D4a) (Fig. 8b), whereas depocentres D5b and D5c are considerably larger than their underlying depocentres (Figs 5b and 7f).

Interpretation. In Santonian times, as large parts of minibasin below depocentres D3a and D3b welded (Fig. 9d), subsidence shifted westwards (Fig. 7e). Thinning of strata towards the minibasin flanks, such as Depocentre D4a, indicates that the subsidence and minibasin formation is under control of sediment loading and salt expulsion underneath, as suggested in previous studies (Hudec et al., 2009). At the same time, the presence of the two small depocentres D4b and D4d directly overlying D3a and D3b suggests that salt withdrawal continued locally (Figs 7e and 8b). As observed in earlier time periods, salt pillows and walls formed as salt became trapped between sub-basins within the subsiding minibasin (e.g. D4c and D5b, which separate Salt Pillow Y from the north-western salt wall; Figs 5a and 8b).

5.4. Eocene to Oligocene

Description. During the interval of the Eocene to Oligocene, minibasin subsidence shifted to the immediate flanks of the adjacent diapirs (Figs 5b and 7g). For example, during the Eocene, Depocentre D6a occurred abruptly in the west of the minibasin and Depocentre D6b progressively grew and extended over early Depocentre D5c towards the east (Figs 7g and 8c). In cross section, depocentres D6a and D6b thicken from the middle of the minibasin of c. 80 ms TWT to minibasin flanks with over 350 ms TWT thick (Fig. 5b). Together, depocentres D6a and D6b define a turtle structure in the south of the minibasin (Fig. 5b). The turtle grew and expanded towards the NE during the Oligocene, as the two Eocene depocentres extended northeastwards to form depocentres

D7a and D7b (Figs 7h and 8c).

Interpretation. The Eocene to Oligocene represents a stage of turtle structure development (Fig. 8c). In Eocene, the turtle structure appeared along Salt Roller Z and later extended along strike forming basinwide turtle structure in Oligocene (Fig. 7a and h). Although turtle structures may be driven by both extension and/or sediment loading (Martin P. A Jackson et al., 1994), we interpret the main control is sediment loading due to the absence of extensional structures (e.g. normal faults) within age-equivalent strata. Moreover, our interpretation is consistent with results arising from the regional study of Valle et al. (2001), who argue thin-skinned extension and related normal faulting had largely ceased by the Eocene times (Valle et al., 2001).

5.5. Miocene to Holocene

Description. During the early Miocene, two depocentres developed above Depocentre D7a on the western side of the minibasin (D8a and D8b; Figs 5b and 7i). By the late Miocene, the minibasin is defined by a single, 4–9 km wide, NE-trending depocentre, the axis of which lies midway between the flanking salt walls (D9; Fig. 7j). Overall, this succession thins towards flanking salt walls, suggesting that the latter were rising at this time (Fig. 5). Subsequent subsidence focused on a single 4–9 km wide, over 600 ms TWT deep depocentre located on the eastern side of the minibasin (D10; Fig. 7k). Depocentre D10 is strongly asymmetrical, thinning towards northwest, as the northwest limb of neighbouring minibasin thrusted over the southwest limb of the studied minibasin with occurrence of vertical salt weld (Fig. 5a).

Interpretation. In Miocene times, subsidence migrated from the west of the minibasin towards the east (Fig. 8d), a shift we infer occurred due to margin tilting and regional contraction. In the early Miocene, margin tilting caused minibasin subsidence in the west so that sediment accumulated preferentially on the western side of the minibasin (D8a and D8b; Fig. 7i). In the late Miocene, contraction affected the intraslope basin area which is evident by the squeezed and uplifted salt walls. Further contraction in Pleistocene was accommodated by thrust and vertical salt weld (Fig. 5a).

6. Discussion

6.1. Depocentre migration during minibasin development

Minibasin initiation and evolution have been studied in considerable detail; early studies generally assumed that minibasin subsidence is driven by its excess density relatively to underlying salt (e.g.

Worrall & Snelson, 1989). Such mechanism is likely to be true during the late stage of minibasin development, when the contained sedimentary sequence is both thick, dense and thus negatively buoyant. It is very unlikely this applies during the initial stage of subsidence when the minibasin is thin and positively buoyant. Based on mechanical considerations, Hudec et al. (2009) suggest a minibasin must be at least 2300 m thick for it to sink under its own weight, although Fernandez et al. (2017) recently suggest that, depending on the composition of the minibasin fill, this value could be less then 1000 m. Instead of density-driven subsidence, a number of other processes that can initiate minibasin formation when the cover strata are still relatively thin; these include thin-skinned extension and contraction (e.g. Brun & Fort, 2011; Ings & Beaumont, 2010), differential loading (e.g. Ge, Jackson, & Vendeville, 1997; Peel, 2014; Bruno C Vendeville, 2005), and thick-skinned and sub-salt deformation (e.g. Hudec et al., 2009; M. P. A Jackson & Vendeville, 1994). However, it is problematic to directly apply these two-dimensional concepts and models to the three-dimensional evolution of natural minibasin.

In this paper, we document the complexity of minibasin growth revealed by the spatial and temporal variability of depocentre development, using variations in stratal unit thickness as a proxy to investigate the minibasin growth, subsidence, and salt migration. The minibasin comprises a succession of depocentres that formed, evolved, and deformed in the space of only a few to tens of kilometres, and over a time interval of several tens of million years. Depocentre initiation occurred due to the onset of normal faulting in the studied area from Cenomanian, under the influence of regional extension (D1; Fig. 4). Then, because the first generation of depocentres (D1) welded to sub-salt strata, the next generation, Turonian depocentre (D2) migrated to areas where salt was still thick and able to flow to create accommodation (Figs 6 and 9). Since the flanking salt walls were relatively high due to the salt inflow, as indicated by the presence of stratal upturn and thinning at the minibasin margins, the new depocentres were forced to migrate along strike (Figs 6 and 10). When the depocentres had welded along the eastern flank of the minibasin, the locus of deposition was forced to shift towards the northwest (Figs 5a, 8b and 9). However, as salt welding was a gradual process, some Santonian depocentres in the east (e.g. D4b and D4d) directly overlay earlier-formed Coniacian depocentres (e.g. D3a and D3b) (Figs 4b, 5 and 6). This process continued as the latest generation of depocentres became welded (Fig. 8c). Only when the contraction took over, did salt welding no longer control depocentre migration. Instead, the transverse migration of depocentres from the Miocene and onwards was controlled by regional tilting and associated thin-skinned contraction (Figs 8d and 9). The complex subsidence history recorded here contrasts with a minibasin growth model envisaging a single, bowl-shaped depocentre that sinks into the salt and finally welds to sub-salt strata (e.g. Hudec et al., 2009; M. P. A Jackson & Vendeville, 1994; Peel, 2014; B. C Vendeville & Jackson, 1992). Instead, for very

large minibasin forming in a kinematically complex setting, where numerous salt bodies and minibasin controls interact, depocentres can progressively migrate or abruptly shift along and across strike; this results in complex minibasin geometries and stratigraphic architectures (Fig. 10).

Previous studies have demonstrated that shifts in depocentre position and minibasin tilting can be controlled by regional contraction (Hudec et al., 2009) or extension (Rowan & Weimer, 1998). However, in the study area, until the Miocene, shifts in depocentre position occurred due to local salt welding, under the influence of extension (Fig. 8a) and/or sedimentary loading (Fig. 8b and c). Similar minibasin subsidence dynamics are observed in Permian minibasins of the Central North Sea (Stewart, 2007, their fig. 4; Stewart & Clark, 1999, their fig. 4b), although in this case, the subsidence is driven by differential loading of dense anhydrite onto less dense halite.

6.2 Salt flow, trapping and welding

A number of studies have focused on salt flow in gravity-driven salt-tectonic systems, showing how salt flows in the dip direction (i.e. slope-parallel direction) (e.g. Brun & Fort, 2011; Cramez & Jackson, 2000; Duval, Cramez, & Jackson, 1992; Hudec & Jackson, 2004; Rowan et al., 2004). Even it has long been known that salt flow and minibasin subsidence are three-dimensional (Rowan, 1993), it is difficult to constrain them in the strike direction. In this study, we were not able to perform three-dimensional halokinetic-sequence analysis (Giles & Rowan, 2012) due to reduced seismic quality immediately adjacent to salt walls and diapirs in areas of steeply dipping strata. As such, we could not precisely constrain how diapir rise rate and sediment accumulation rate varied both through time and, critically in the context of the along-strike dynamics documented here, through space. However, the patterns of depocentre migration we have identified in the study area suggest the flow of salt between different salt bodies was spatially and temporarily variable. For example, from the Cenomanian to Turonian, as the locus of deposition migrated southwards from D1 to D2b, the salt wall rise started first in the northeast of the minibasin and then towards the south (Figs 4b and 8a). The salt wall in the west formed even later, after major depocentres shifted to the west in the Santonian (Fig. 9e).

Our study also shows that a salt pillow or salt-cored anticline can simply be remnant salt trapped in the anticline due to depocentre migration and accompanied three-dimensional salt flow, and not the result of turtle formation. A recent study has suggested that salt-cored anticline related to the formation of turtle structures, as the minibasin flanks subside quicker than the centre and trap the underlying salt (Peel, 2014). In the study area, Salt Pillow Y was not formed by a single stage of depocentre welding, nor by the formation of a turtle structure, but through progressive welding of multiple depocentres (Fig. 3b). In essence, the northeastern, southern and western

boundaries of Salt Pillow Y formed through salt welding in Turonian, Cenomanian and Santonian to Paelocene times respectively (Fig. 8).

A phenomenon that accompanies the migration of depocentres and progressive formation of salt pillows is the diachronous welding of salt, an observation that has been made at the regional scale (Roberts, Metzgar, Liu, & Lim, 2004). Our study however demonstrates that even within a single minibasin, the timing of salt welding is likely to be diachronous and spatially complex due to the ever-shifting locations of subsidence. Such process of protracted welding of tens of million years contrasts remarkably to the one-off salt welding of a minibasin suggested by current, largely two-dimensional models (e.g. Peel, 2014; B. C Vendeville & Jackson, 1992).

7. Conclusions

Our interpretation of high quality seismic reflection data from an intraslope minibasin in the Lower Congo Basin permits a detailed analysis of structural and stratigraphic evolution of the minibasin development and related salt flow. Interpreting closely-spaced horizons allows us to develop a high resolution tectono-stratigraphic framework that reveals, in some detail, a history of depocentre and subsidence migration, salt trapping and salt welding.

The time-thickness maps show the minibasin in this study is the result of amalgamation of multiple depocentres. We identify four stages of depocentre migration plus a pre-kinematic stage of Albian: 1. Depocentre initiation and lateral migration under extension from Cenomanian to Coniacian; 2. Transverse shift of depocentres to the west under the control of sedimentary loading from Santonian to Paleocene; 3. Turtle structure formation under sedimentary loading from Eocene to Oligocene; 4. Transverse migration of depocentres under regional tilting and contraction.

Our analysis of the minibasin has allowed us to identify the driven force for minibasin growth. The early initiation and lateral migration of depocentres within the minibasin are largely controlled by the extension. However, the exact timing and location of depocentre shift are closely linked to the salt flow and weld. As early depocentres weld on sub-salt strata, late depocentres are forced to migrate to places where salt withdraw is ongoing and creating accommodation space. In contrast, after the minibasin has largely welded, later contraction squeezes the salt walls and creates salt highs, forcing the depocentres to migrate to topographic lows within the minibasin. Moreover, the shift of depocentre location and subsequently salt welding also result in complex salt flow which in turn play a significant role in formation of salt-related structures. The trapping of the remnant salt by diachronous salt welding forms salt pillows underneath the minibasin in a span of more than 70 Myr.

This study demonstrates that a single minibasin is the result of three-dimensional depocentre

migration and salt flow. Consequently, current models of minibasin growth need to revise to take into account the spatial and temporal variations of minibasin geometries and stratigraphy. Moreover, the shifting of depocentre locations also provides a framework for understanding the associated sedimentary systems and facies distributions within the minibasins.

Acknowledgements

This study was supported by Equinor. We acknowledge PGS for providing access to seismic data and giving permission to publish the seismic sections in this paper. Schlumberger is thanked for providing the Petrel software in the 3D Seismic Lab at the University of Bergen.

References

Anderson, J. E., Cartwright, J., Drysdall, S. J., & Vivian, N. (2000). Controls on turbidite sand deposition during gravity-driven extension of a passive margin: examples from Miocene sediments in Block 4, Angola. *Marine and Petroleum Geology, 17*(10), 1165–1203.

Anka, Z., & Séranne, M. (2004). Reconnaissance study of the ancient Zaire (Congo) deep-sea fan.(ZaiAngo Project). *Marine Geology, 209*(1), 223–244.

Barde, J.-P., Chamberlain, P., Galavazi, M., Harwijanto, J., Marsky, J., Gralla, P., & van den Belt, F. (2002). Sedimentation during halokinesis: Permo-Triassic reservoirs of the Saigak field, Precaspian basin, Kazakhstan. *Petroleum Geoscience, 8*(2), 177–187.

Birch, F. (1960). The velocity of compressional waves in rocks to 10 kilobars: 1. *Journal of Geophysical Research, 65*(4), 1083–1102. doi:doi:10.1029/JZ065i004p01083

Brun, J.-P., & Fort, X. (2011). Salt tectonics at passive margins: Geology versus models. *Marine and Petroleum Geology, 28*(6), 1123–1145.

Callot, J.-P., Salel, J.-F., Letouzey, J., Daniel, J.-M., & Ringenbach, J.-C. (2016). Three-dimensional evolution of salt-controlled minibasins: Interactions, folding, and megaflap development. *AAPG Bulletin, 100*(9), 1419–1442.

Clark, J., Stewart, S., & Cartwright, J. (1998). Evolution of the NW margin of the North Permian Basin, UK North Sea. *Journal of the Geological Society, London, 155*(4), 663-676.

Cramez, C., & Jackson, M. P. A. (2000). Superposed deformation straddling the continental-oceanic transition in deep-water Angola. *Marine and Petroleum Geology, 17*(10), 1095–1109.

Duffy, O. B., Fernandez, N., Hudec, M. R., Jackson, M. P., Burg, G., Dooley, T. P., & Jackson, C. A.-L. (2017). Lateral mobility of minibasins during shortening: Insights from the SE Precaspian Basin, Kazakhstan. *Journal of Structural Geology, 97*, 257–276.

Duval, B., Cramez, C., & Jackson, M. P. A. (1992). Raft tectonics in the Kwanza basin, Angola. *Marine and Petroleum Geology, 9*(4), 389–404.

Fernandez, N., Duffy, O. B., Hudec, M. R., Jackson, M. P. A., Burg, G., Jackson, C. A. L., & Dooley, T. P. (2017). The origin of salt-encased sediment packages: Observations from the SE Precaspian Basin (Kazakhstan). *Journal of Structural Geology, 97*, 237–256. doi:https://doi.org/10.1016/j.jsg.2017.01.008

Fort, X., Brun, J.-P., & Chauvel, F. (2004). Salt tectonics on the Angolan margin, synsedimentary deformation processes. *AAPG Bulletin, 88*(11), 1523–1544.

Ge, H., Jackson, M. P., & Vendeville, B. C. (1997). Kinematics and dynamics of salt tectonics driven by progradation. *AAPG Bulletin, 81*(3), 398–423.

Giles, K. A., & Rowan, M. G. (2012). Concepts in halokinetic-sequence deformation and stratigraphy. *Geological Society, London, Special Publications, 363*(1), 7–31.

Goteti, R., Ings, S. J., & Beaumont, C. (2012). Development of salt minibasins initiated by sedimentary topographic relief. *Earth and Planetary Science Letters, 339–340*, 103–116. doi:http://dx.doi.org/10.1016/j.epsl.2012.04.045

Hodgson, N. A., Farnsworth, J., & Fraser, A. J. (1992). Salt-related tectonics, sedimentation and hydrocarbon plays in the Central Graben, North Sea, UKCS. *Geological Society, London, Special Publications, 67*(1), 31–63.

Hudec, M. R., & Jackson, M. P. (2004). Regional restoration across the Kwanza Basin, Angola: Salt tectonics triggered by repeated uplift of a metastable passive margin. *AAPG Bulletin, 88*(7), 971–990.

Hudec, M. R., & Jackson, M. P. A. (2007). Terra infirma: Understanding salt tectonics. *Earth-Science Reviews, 82*(1), 1–28.

Hudec, M. R., Jackson, M. P. A., & Schultz-Ela, D. D. (2009). The paradox of minibasin subsidence into salt: Clues to the evolution of crustal basins. *Geological Society of America Bulletin, 121*(1-2), 201–221.

Hudec, M. R., Jackson, M. P. A., Vendeville, B. C., Schultz-Ela, D. D., & Dooley, T. P. (2011). The salt mine: A digital atlas of salt tectonics.

Ings, S. J., & Beaumont, C. (2010). Shortening viscous pressure ridges, a solution to the enigma of initiating salt 'withdrawal'minibasins. *Geology, 38*(4), 339–342.

Jackson, C. A.-L., Rodriguez, C. R., Rotevatn, A., & Bell, R. E. (2014). Geological and geophysical expression of a primary salt weld: An example from the Santos Basin, Brazil. *Interpretation, 2*(4), SM77–SM89.

Jackson, M. P., & Talbot, C. J. (1991). *A glossary of salt tectonics*: Bureau of Economic Geology, University of Texas at Austin.

Jackson, M. P. A., & Cramez, C. (1989). *Seismic recognition of salt welds in salt tectonics regimes.* Paper presented at the Gulf of Mexico salt tectonics, associated processes and exploration potential: Gulf Coast Section SEPM Foundation 10th Annual Research Conference.

Jackson, M. P. A., & Hudec, M. R. (2017). *Salt tectonics: Principles and practice*: Cambridge University Press.

Jackson, M. P. A., & Vendeville, B. C. (1994). Regional extension as a geologic trigger for diapirism. *Geological Society of America Bulletin, 106*(1), 57A systematic technique for the sequential restoration of salt structures73.

Jackson, M. P. A., Vendeville, B. C., & Schultz-Ela, D. D. (1994). Structural dynamics of salt systems. *Annual Review of Earth and Planetary Sciences, 22*, 93–117.

Lamb, M. P., Toniolo, H., & Parker, G. (2006). Trapping of sustained turbidity currents by intraslope minibasins. *Sedimentology, 53*(1), 147–160.

Lavier, L. L., Steckler, M. S., & Brigaud, F. (2001). Climatic and tectonic control on the Cenozoic evolution of the West African margin. *Marine Geology, 178*(1–4), 63–80.

Marsh, N., Imber, J., Holdsworth, R. E., Brockbank, P., & Ringrose, P. (2010). The structural evolution of the Halten Terrace, offshore Mid‐Norway: extensional fault growth and strain localisation in a multi‐layer brittle–ductile system. *Basin Research, 22*(2), 195–214.

Marton, G., Tari, G. C., & Lehmann, C. T. (2000). Evolution of the Angolan Passive Margin, West Africa, With Emphasis on Post‐Salt Structural Styles. *Geophysical Monograph-American Geophysical Union*(115), 129–149.

McBride, B. C., Rowan, M. G., & Weimer, P. (1998). The evolution of allochthonous salt systems, northern Green Canyon and Ewing Bank (offshore Louisiana), northern Gulf of Mexico. *AAPG Bulletin, 82*(5), 1013–1036.

Nürnberg, D., & Müller, R. D. (1991). The tectonic evolution of the South Atlantic from Late Jurassic to present. *Tectonophysics, 191*(1), 27–53.

Oluboyo, A. P., Gawthorpe, R. L., Bakke, K., & Hadler‐Jacobsen, F. (2014). Salt tectonic controls on deep‐water turbidite depositional systems: Miocene, southwestern Lower Congo Basin, offshore Angola. *Basin Research, 26*(4), 597–620.

Peel, F. J. (2014). How do salt withdrawal minibasins form? Insights from forward modelling, and implications for hydrocarbon migration. *Tectonophysics, 630*, 222–235.

Prather, B. E., Booth, J. R., Steffens, G. S., & Craig, P. A. (1998). Classification, lithologic calibration, and stratigraphic succession of seismic facies of intraslope basins, deep-water Gulf of Mexico. *AAPG Bulletin, 82*(5), 701–728.

Quirk, D. G., Schødt, N., Lassen, B., Ings, S. J., Hsu, D., Hirsch, K. K., & Von Nicolai, C. (2012). Salt tectonics on passive margins: examples from Santos, Campos and Kwanza basins. *Geological Society, London, Special Publications, 363*(1), 207–244.

Roberts, M. J., Metzgar, C. R., Liu, J., & Lim, S. J. (2004). Regional assessment of salt weld timing, Campos Basin, Brazil. In P. J. Post, D. L. Olson, K. T. Lyons, S. L. Palmes, P. F. Harrison, & N. C. Rosen (Eds.), *Salt-Sediment Interactions and Hydrocarbon Prospectivity: Concepts, Applications, and Case Studies for the 21st Century.* (pp. 371–389). Houston: Society of Economic Paleontologist and Mineralogists, Gulf Coast Section.

Rowan, M. G. (1993). A systematic technique for the sequential restoration of salt structures. *Tectonophysics, 228*(3–4), 331–348.

Rowan, M. G., Lawton, T. F., & Giles, K. A. (2012). Anatomy of an exposed vertical salt weld and flanking strata, La Popa Basin, Mexico. *Geological Society, London, Special Publications, 363*(1), 33–57.

Rowan, M. G., Peel, F. J., & Vendeville, B. C. (2004). Gravity-driven fold belts on passive margins. In K. R. McClay (Ed.), *AAPG Memoir* (Vol. 82, pp. 157–182).

Rowan, M. G., & Weimer, P. (1998). Salt-sediment interaction, northern Green Canyon and Ewing bank (offshore Louisiana), northern Gulf of Mexico. *AAPG Bulletin, 82*(5), 1055–1082.

Stewart, S. A. (2007). Salt tectonics in the North Sea Basin: a structural style template for seismic interpreters. In A. C. Ries, R. W. H. Butler, & R. H. Graham (Eds.), *Geological Society of London, Special Publication* (Vol. 272, pp. 361–396).

Stewart, S. A., & Clark, J. A. (1999). *Impact of salt on the structure of the Central North Sea hydrocarbon fairways.* Paper presented at the Geological Society, London, Petroleum Geology Conference series.

Trudgill, B. D. (2011). Evolution of salt structures in the northern Paradox Basin: controls on evaporite deposition, salt wall growth and supra-salt stratigraphic architecture. *Basin Research, 23*(2), 208–238. doi:10.1111/j.1365-2117.2010.00478.x

Valle, P. J., Gjelberg, J. G., & Helland-Hansen, W. (2001). Tectonostratigraphic development in the eastern Lower Congo Basin, offshore Angola, west Africa. *Marine and Petroleum Geology, 18*(8), 909–927.

Vendeville, B. C. (2005). Salt tectonics driven by sediment progradation: Part I—Mechanics and kinematics. *AAPG Bulletin, 89*(8), 1071–1079.

Vendeville, B. C., & Jackson, M. P. A. (1992). The fall of diapirs during thin-skinned extension. *Marine and Petroleum Geology, 9*(4), 354–371.

Wagner, B. H. (2010). *An analysis of salt welding.* (PhD), University of Texas at Austin,

Wagner, B. H., & Jackson, M. P. A. (2011). Viscous flow during salt welding. *Tectonophysics, 510*(3), 309–326.

Warsitzka, M., Kley, J., & Kukowski, N. (2013). Salt diapirism driven by differential loading — Some insights from analogue modelling. *Tectonophysics, 591*, 83–97. doi:https://doi.org/10.1016/j.tecto.2011.11.018

Worrall, D. M., & Snelson, S. (1989). Evolution of the northern Gulf of Mexico, with emphasis on Cenozoic growth faulting and the role of salt. In A. W. Bally & A. R. Palmer (Eds.), *The Geology of North America-An Overview* (pp. 97–137).

FIGURE CAPTIONS

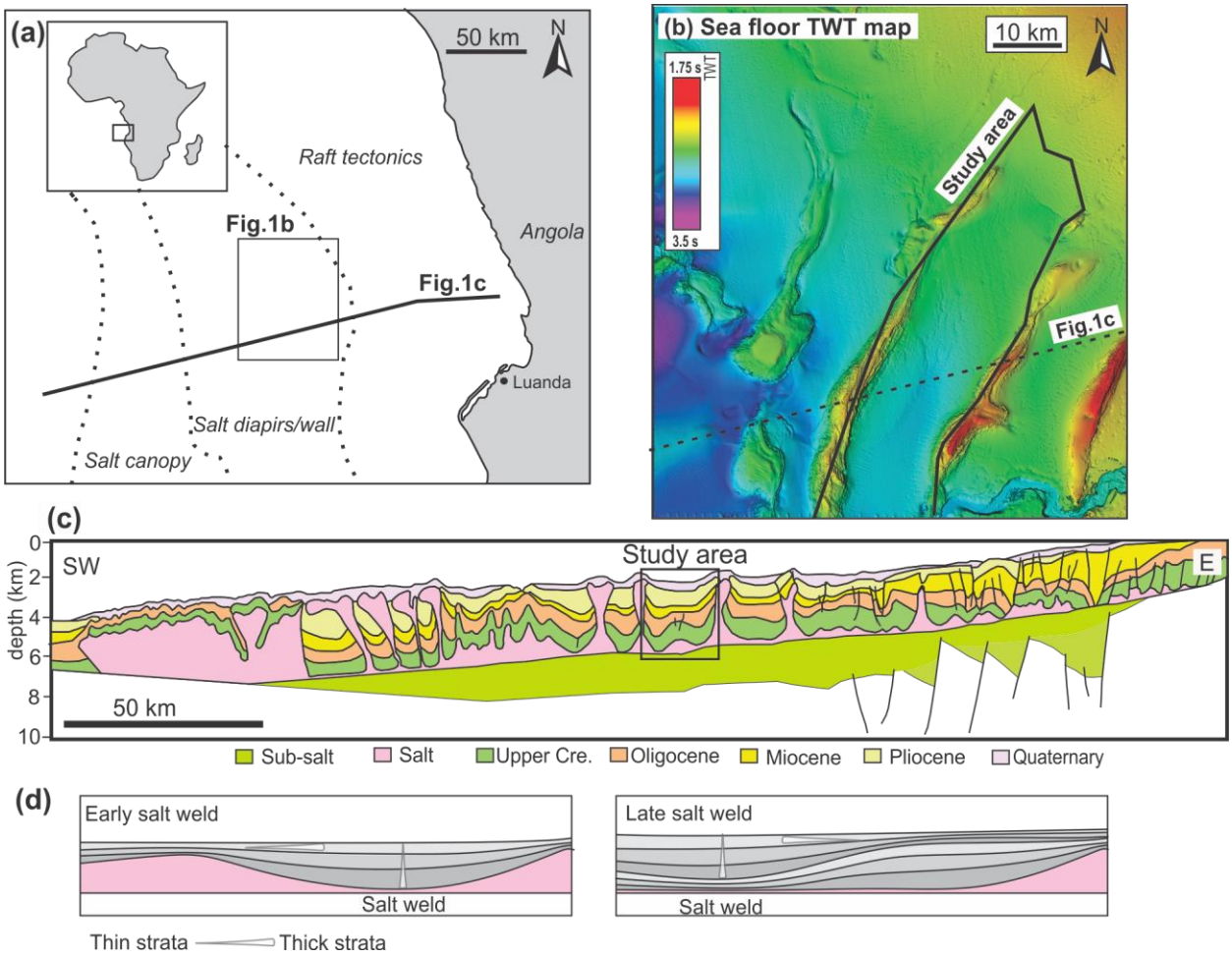

Figure 1. (a) Simplified map showing the location and structural domains of the Lower Congo Basin (modified after Marton et al., 2000). The dotted lines are domain boundaries. Inset shows the geographical location of the Lower Congo Basin. (b) Seafloor TWT map of the intraslope area of the Lower Congo Basin. The salt walls and diapirs are visible as local bathymetric highs. The location is shown in (a). (c) Regional profile of the Lower Congo Basin (modified after Marton et al., 2000). Note the thin-skinned, upslope extension and downslope contraction system developed above the salt. Approximate location of the study area is indicated. The location of the profile is shown in (a) and (b). (d) Schematic diagram showing the stratal architecture during progressive salt welding (modified from Jackson & Hudec, 2017). Note the vertical and lateral thickness variations of strata during the depocentre shift.

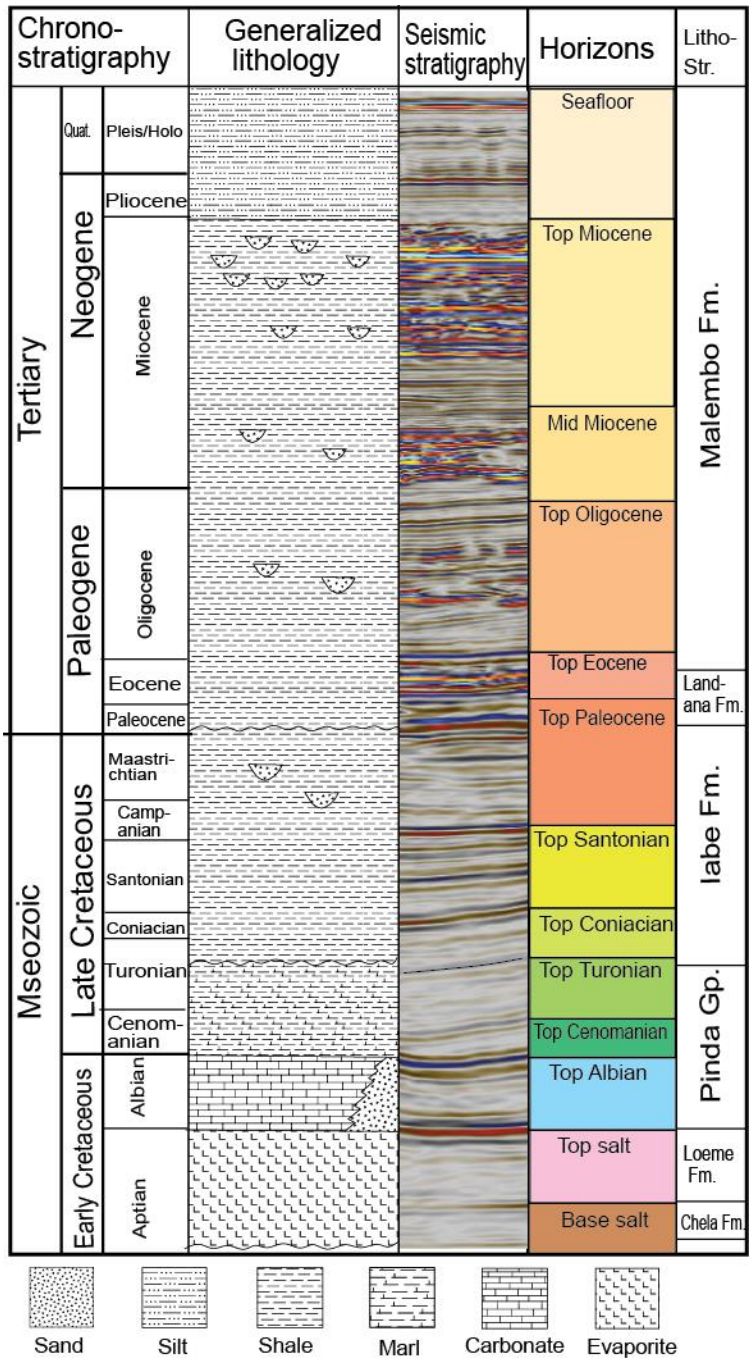

562

563 **Figure 2.** Stratigraphy of the Lower Congo Basin and interpreted horizons (modified after
564 Anderson et al., 2000; Valle et al., 2001).

565

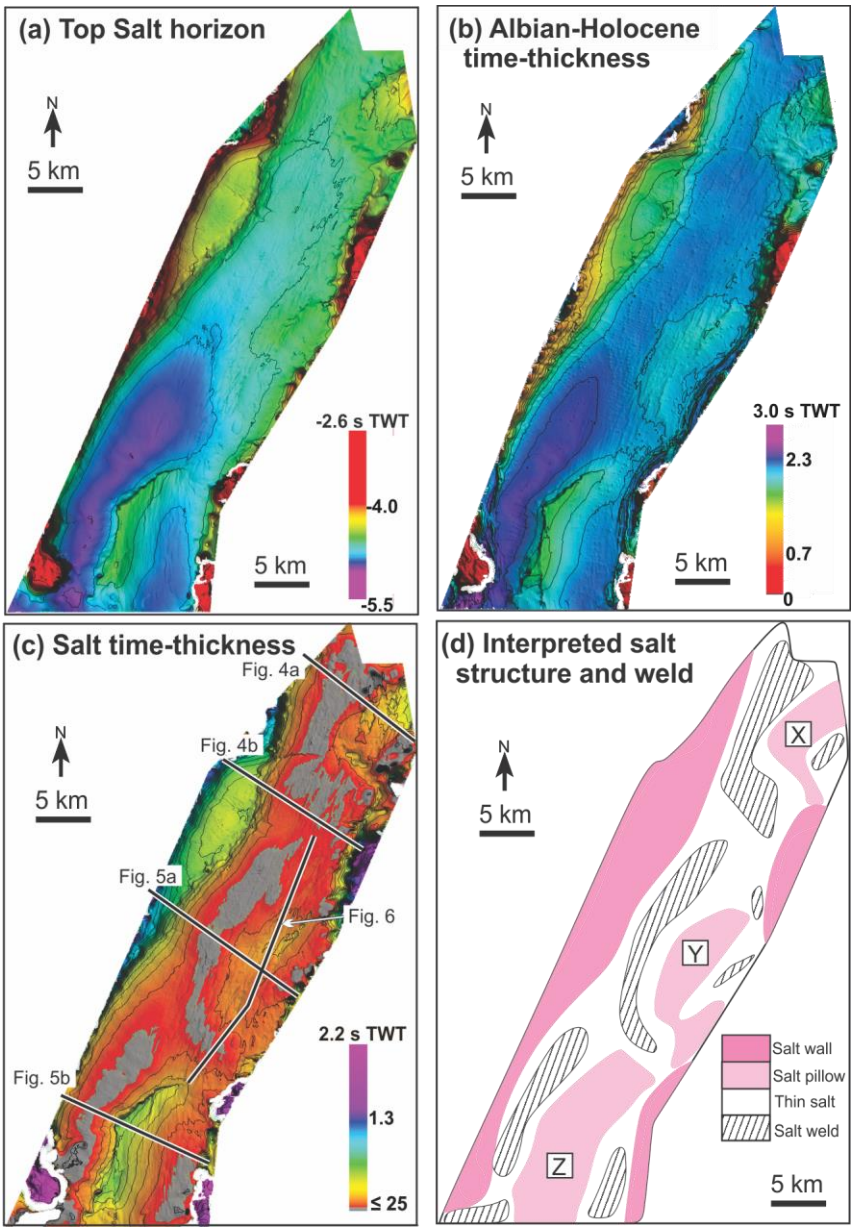

Figure 3. TWT structure and time-thickness maps of the salt and supra-salt cover strata of the intraslope minibasin. (a) TWT structure map of the top salt horizon illustrating highs and lows of salt-related structures within the present-day minibasin. (b) Supra-salt cover time-thickness showing the thickness variations within the cover strata. Note that the thin supra-salt areas are thick salt areas in (c). (c) Salt time-thickness map, and its simplified sketch (d) showing the location of salt welds (<25 ms TWT) and salt walls/diapir. Note the three salt pillows X, Y and Salt Roller Z, located within the present-day minibasin.

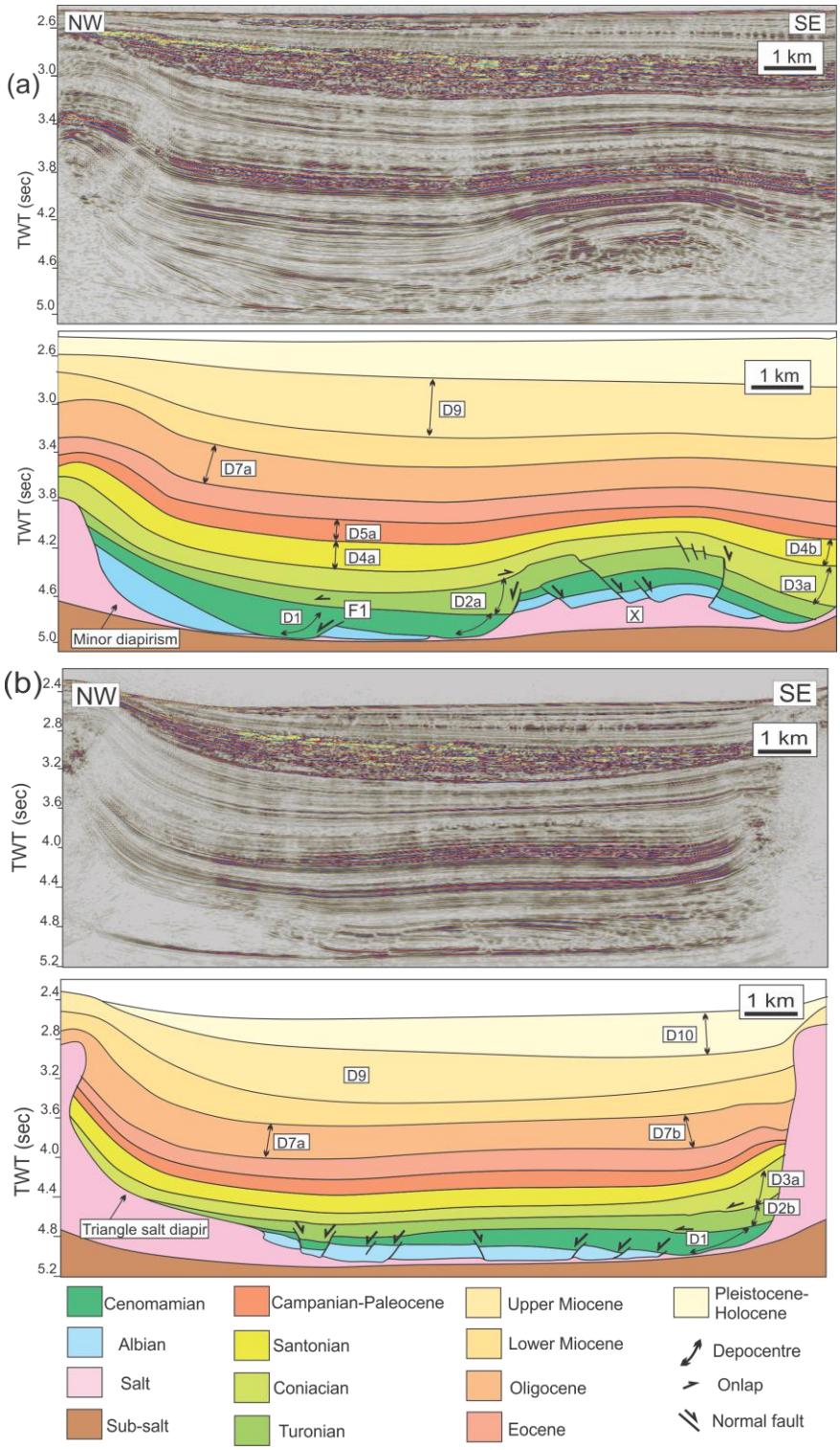

Figure 4. Seismic section and interpretation of the northernmost part of the minibasin. (a) Seismic section (above) and interpretation (below) illustrate the structural style and stratigraphic architecture in the north of the minibasin. X is a salt pillow referred to in the text. D1 to D9 are depocentres referred to in the text. Note the growth strata of D1 and D2a along normal faults. For section location, see Figs 3c and 7a. (b) Seismic section (above) and interpretation (below) illustrating the structural style and stratigraphic architecture of the northern part of the minibasin, southwest of the line of Fig. 4a. Note the growth strata of depocentres D1, D2b and D3a. D1, D2b, D3a, D7a, D7b, D9 and D10 are depocentres referred in the main text. For section location, see Figs 3c and 7a.

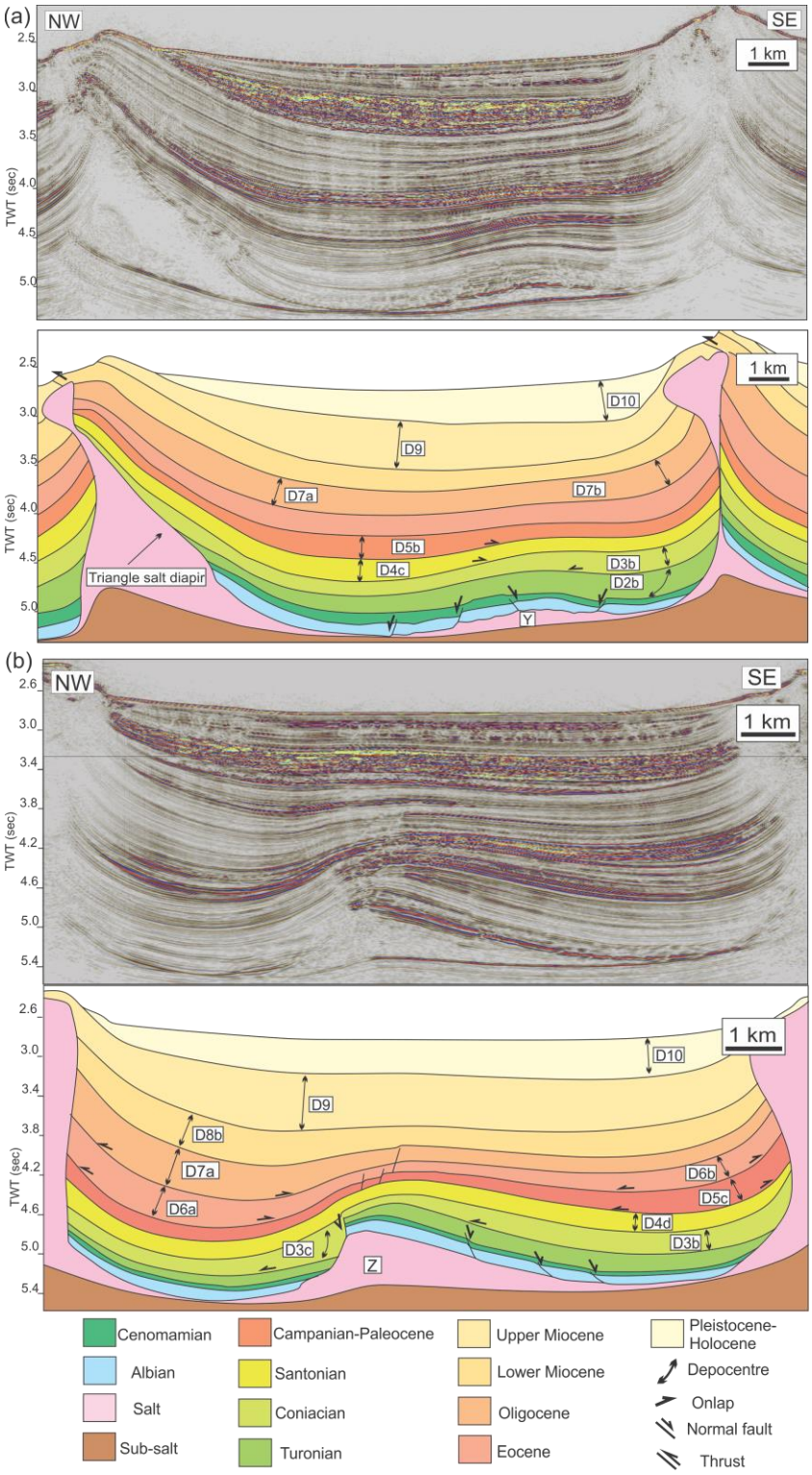

Figure 5. Seismic section and interpretation of the central and southern part of the present-day minibasin. (a) Seismic section (above) and interpretation (below) illustrate the structural style and stratigraphic architecture in the central part of the minibasin. Y is a salt pillow referred in the text. D2a to D10 are depocentres referred to in the text. For section location, see Figs 3c and 7a. (b) Seismic section (above) and interpretation (below) illustrating the structural style and stratigraphic architecture of the southern part of the minibasin. Note the normal fault-bounded depocentre D3c. D3b, D3c, D5c, D6a, D6b, D7a, D8b, D9 and D10 are depocentres referred in the main text. Z is a salt roller referred in the text. For section location, see Figs 3c or 7a.

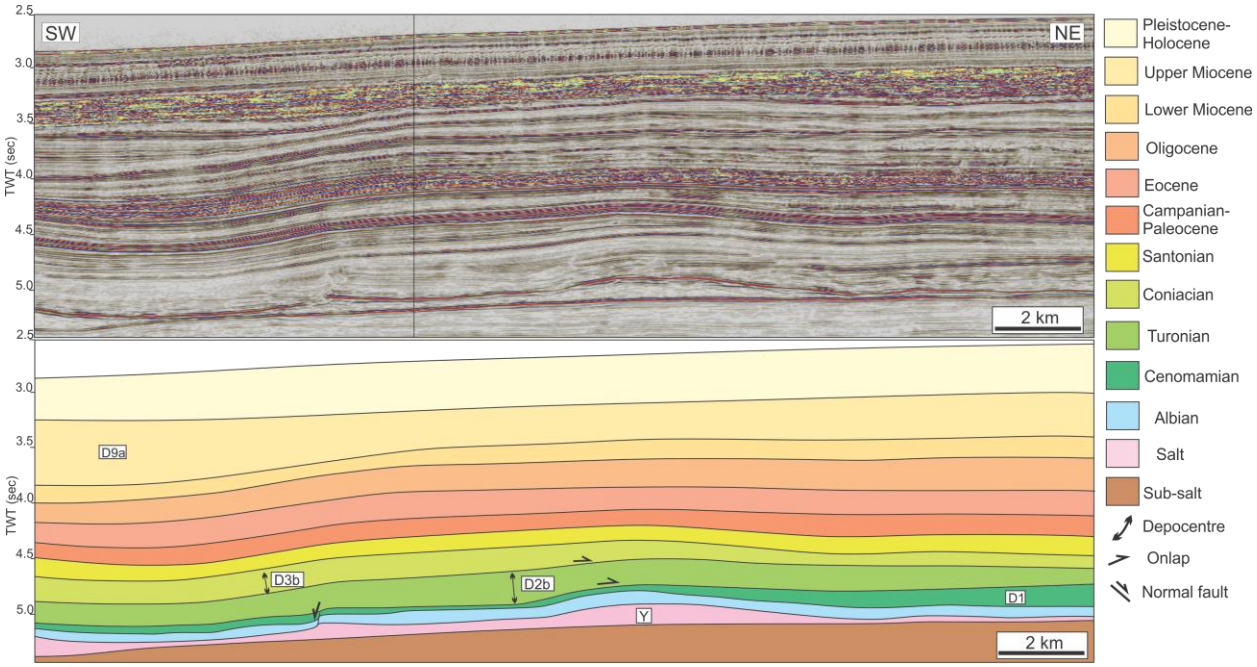

Figure 6. Seismic section (above) and interpretation (below) illustrating the structural style and stratigraphic architecture along the strike of the minibasin. Note the onlap from D3a to D2b and from D2b to D1 respectively. D1, D2b, D3a and D9 are depocentres referred to in the text. Y is a salt pillow referred in the text. For section location, see Figs 3c or 7c.

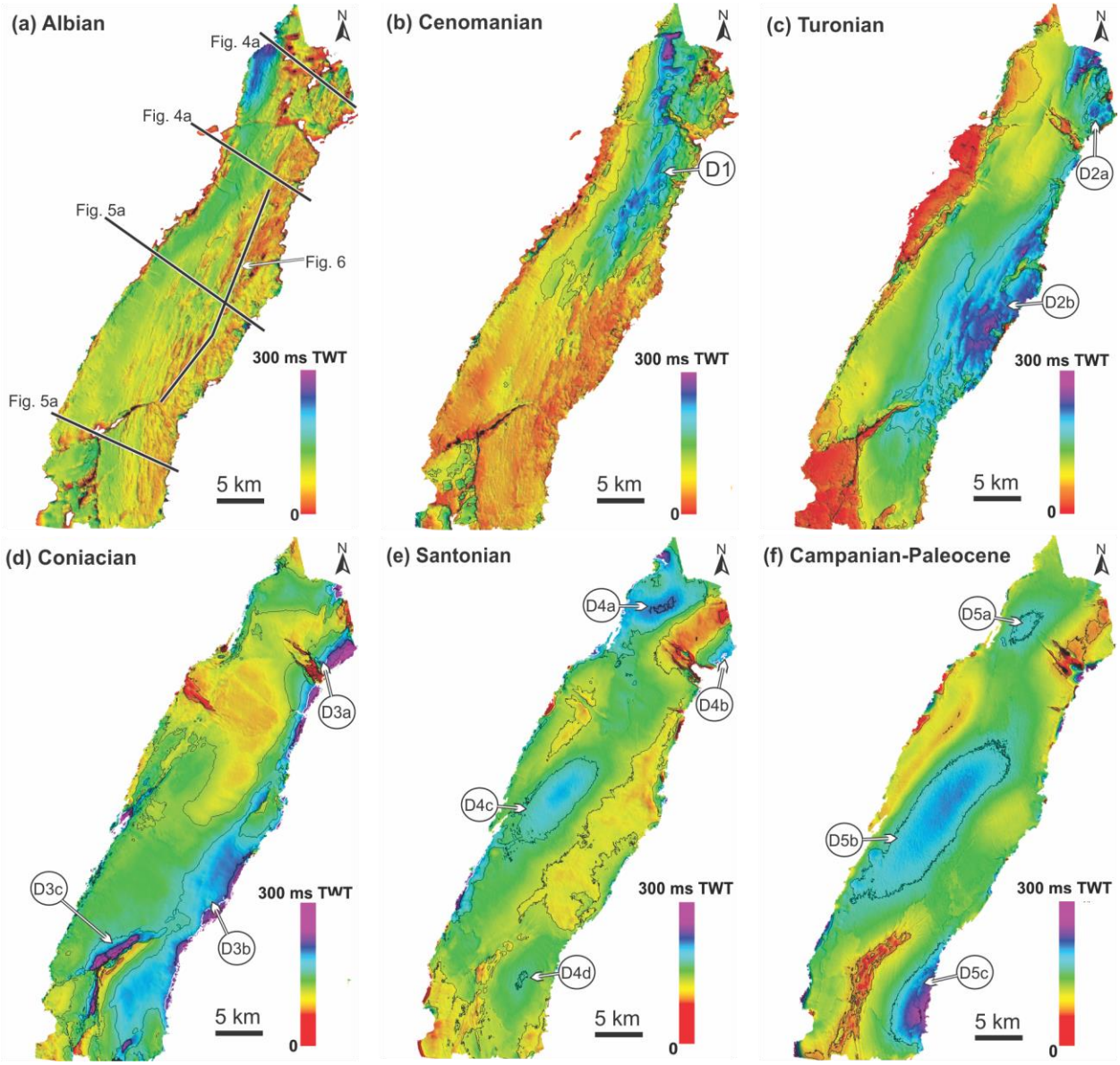

Figure 7. Time-thickness maps for each of the nine supra-salt units considered in this study. (a) Albian: limited thickness variations, indicating a quiescent stage. (b) Cenomanian: widespread small normal faults and the development of depocentre D1 controlled by normal faults. (c) Turonian: lateral migration of depocentres D2a and D2b. Depocentre D2b develops southwards of but overlaps depocentre D1. (d) Coniacian: migration of depocentres D3a, D3b and D3c. (e) Santonian: development of new depocentres (D4a and D4c) to the west of the old depocentres (D4b and D4d), which remain active. (f) Campanian–Paleocene: growth of depocentres D5a, D5b and D5c.

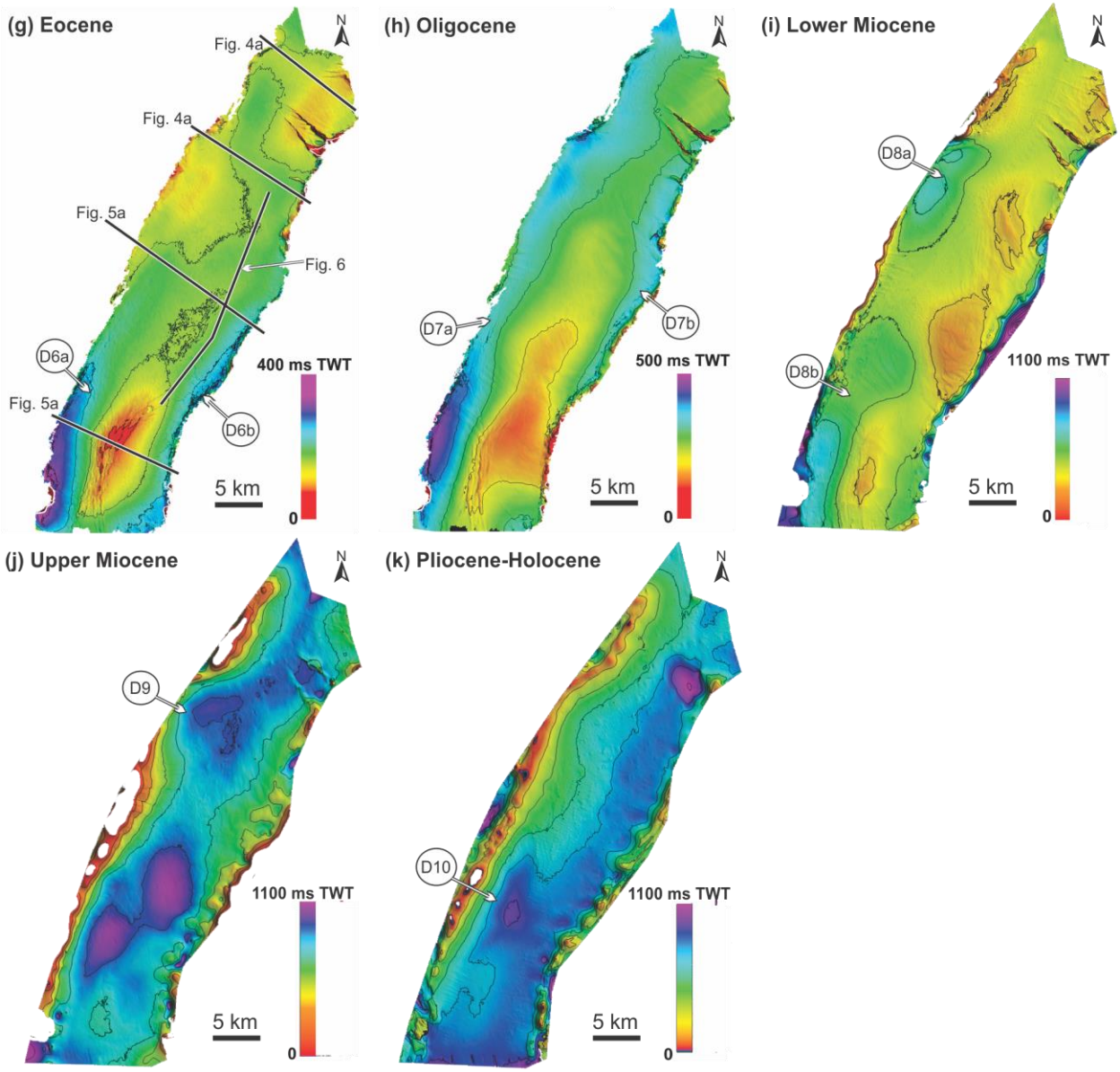

610

611 **Figure 7. Continued** (g) Eocene: development of depocentres D6a and D6b along the flanks of
612 the minibasin. (h) Oligocene: growth and migration of depocentres of D7a and D7b in a northward
613 direction. (i) Early Miocene: newly developed depocentres D8a and D8a migrate to the west of
614 the minibasin. (j) Later Miocene: elongate depocentre D9 in centre of the minibasin. (k)
615 Pleistocene to Holocene: depocentre D10 in east of the minibasin.

616

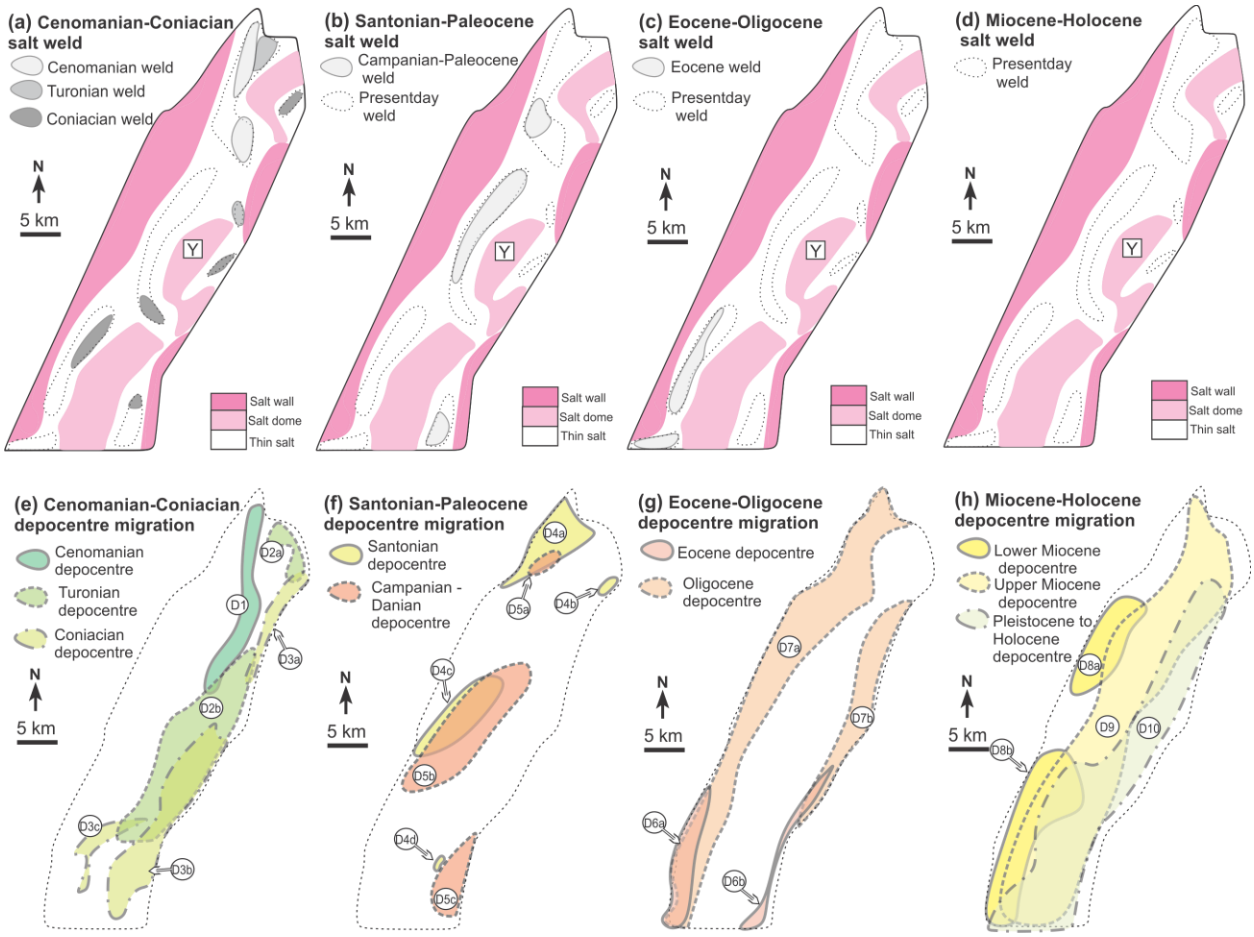

Figure 8. Schematic diagram illustrating the four stages of depocentre migration and interpreted concurrent evolution of the salt weld in the minibasin. Locations and sequences of salt weld: (a) During depocentre lateral migration, from Cenomanian to Coniacian; (b) From Santonian to Paleocene; (c) From Eocene to Oligocene, during turtle structure formation. (d) No further salt weld on sub-salt strata from Miocene to Holocene. (e) Initiation of first depocentre and subsequent lateral depocentre migration from Cenomanian to Coniacian. (f) Depocentres shift and growth to the west of early formed depocentres from Santonian to Paleocene. (g) Migration of depocentres to the flanks of the minibasin and formation of turtle structure from Eocene to Miocene. (h) Migration of depocentres from the west of the minibasin to the east due to margin tilting and contraction.

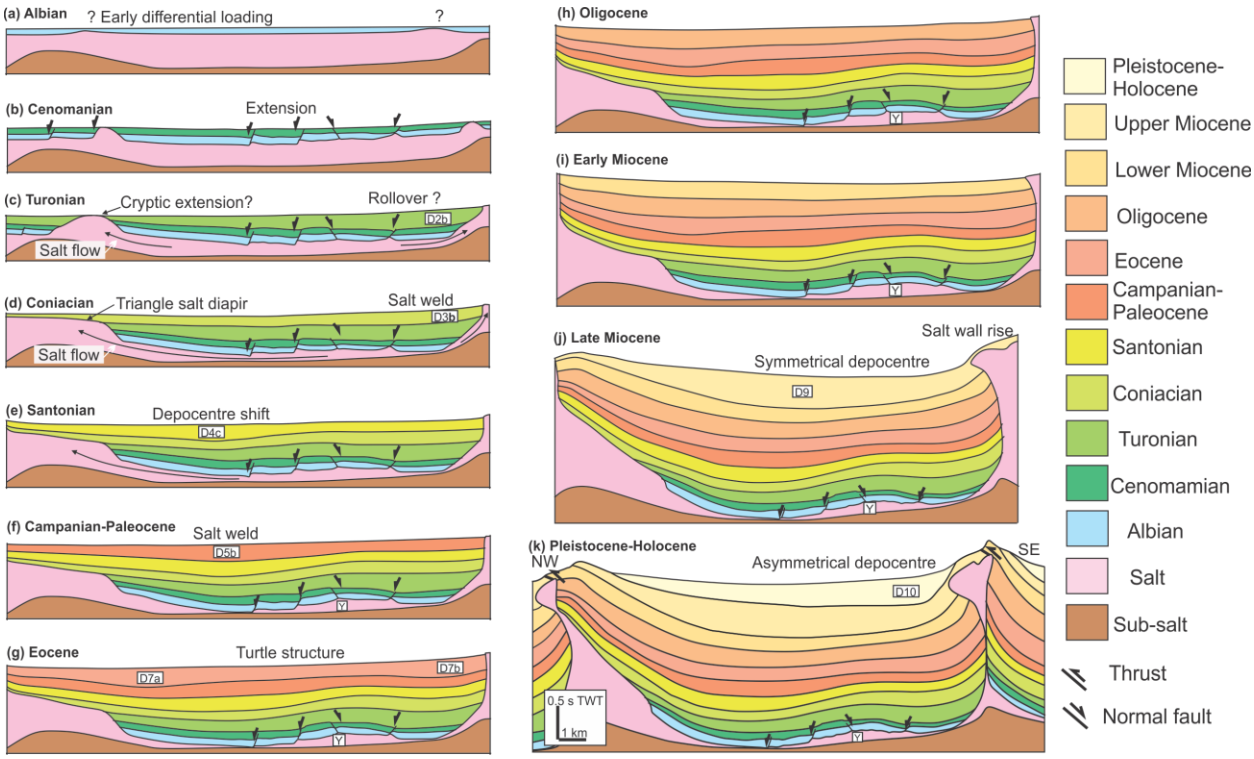

Figure 9. Schematic diagram based on Fig. 5a illustrating depocentre migration in the central part of the minibasin. (a) Albian is a relatively quiescent stage. (b)-(d) Cenomanian to Coniacian: depocentre migrated under extension, note the growth strata of depocentre D2a and salt weld occurred before depocentre D3a. (e)-(f) Santonian to Paleocene: deposition shifted to the west of the minibasin. (g)-(h) Eocene: turtle structure developed as centres of deposition formed on both sides of the minibasin. (i)-(k) Miocene to Holocene: depocentres migrated towards southeast due to elevated salt diapir/wall. See text for discussion.

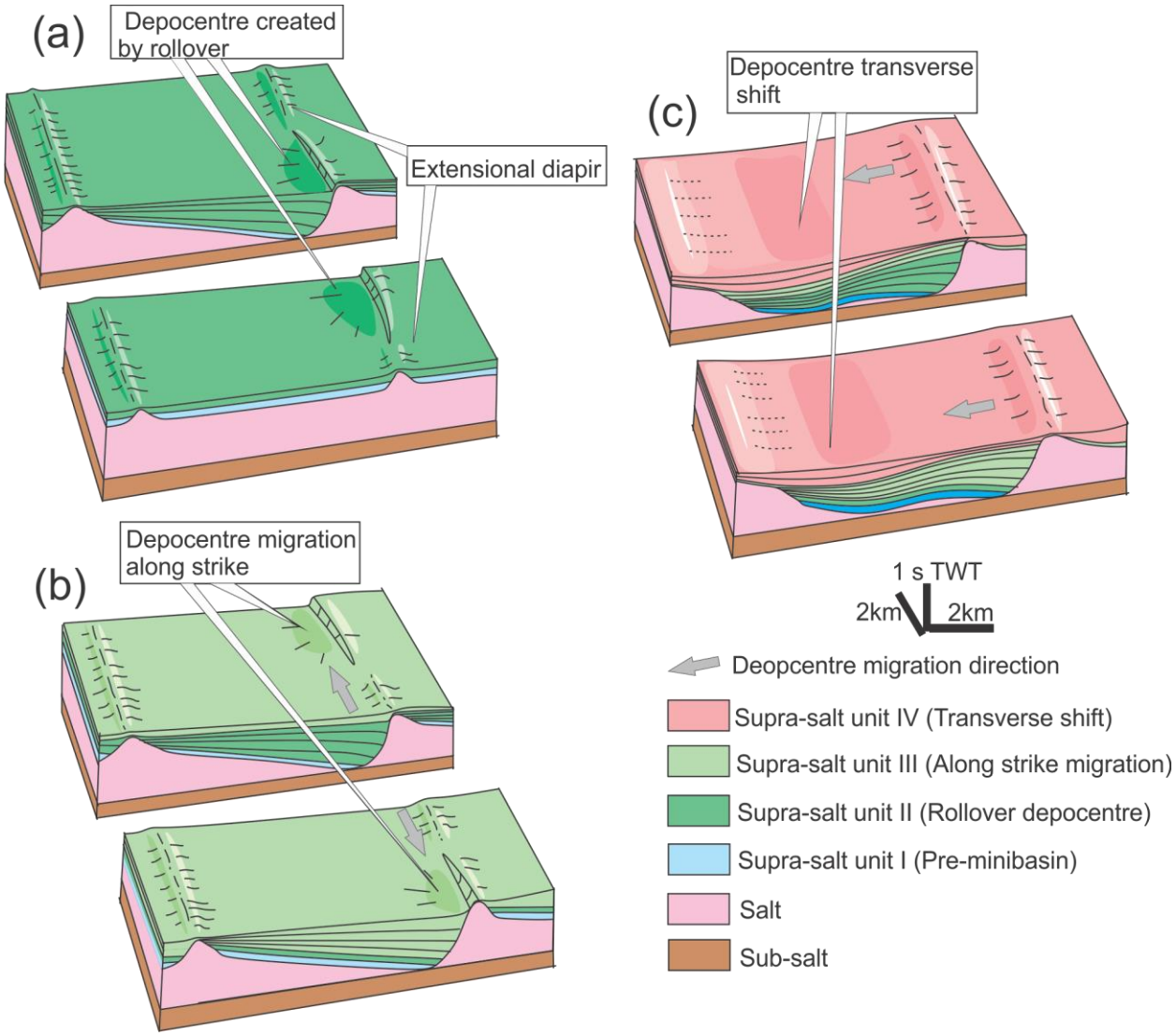

638

639 **Figure 10.** Block diagram illustrating the along-strike migration and transverse shift of
640 depocentres and related salt weld within a single minibasin. (a) Minibasin initiation by
641 extensional depocentre. (b) Depocentre along-strike migration due to salt weld and continued
642 extension. (c) Depocentre shift to across the minibasin axis due to salt weld. Note the formation
643 of underlying salt pillow is irrelevant to turtle structure.